

# Giant optical nonlinearity of a single plasmonic nanostructure

Pavel N. Melentiev,<sup>1</sup> Anton E. Afanasiev,<sup>1</sup> Artur A. Kuzin,<sup>2</sup> Andrey S. Baturin,<sup>2</sup>  
and Victor I. Balykin<sup>1,\*</sup>

<sup>1</sup>*Institute for Spectroscopy Russian Academy of Sciences, Moscow, Troitsk, Fizicheskaya str. 5, 142190, Russia*

<sup>2</sup>*Moscow Institute of Physics and Technology, Dolgoprudny, Moscow reg., 141700, Russia*

\*[balykin@isan.troitsk.ru](mailto:balykin@isan.troitsk.ru)

**Abstract:** We realize giant optical nonlinearity of a single plasmonic nanostructure which we call a split hole resonator (SHR). The SHR is the marriage of two basic elements of nanoplasmonics, a nanohole and a nanorod. A peak field intensity in the SHR occurs at the *single* tip of the nanorod inside the nanohole. The peak field is much stronger than those of the nanorod and nanohole, because the SHR field involves contributions from the following two field-enhancement mechanisms: (1) the excitation of surface plasmon resonances and (2) the lightning-rod effect. Here, we demonstrate the use of the SHR as a highly efficient nonlinear optical element for: (i) the generation of the third harmonic from a single SHR; (ii) the excitation of intense multiphoton luminescence from a single SHR.

©2013 Optical Society of America

**OCIS codes:** (310.6628) Subwavelength structures, nanostructures; (050.1220) Apertures; (350.4238) Nanophotonics and photonic crystals; (310.4165) Multilayer design; (260.2710) Inhomogeneous optical media; (190.2620) Harmonic generation and mixing.

---

## References and links

1. S. A. Maier, *Plasmonics: Fundamentals and Applications* (Springer, 2007).
2. V. M. Shalaev and S. Kawata, eds., *Nanophotonics with Surface Plasmons* (Elsevier, 2007).
3. M. L. Brongersma and P. G. Kik, eds., *Surface Plasmon Nanophotonics, Series: Springer Series in Optical Sciences* (Springer, 2007, Vol. 131).
4. A. E. Neeves and M. H. Birnboim, "Composite structures for the enhancement of nonlinear-optical susceptibility," *J. Opt. Soc. Am. B* **6**(4), 787 (1989).
5. R. D. Averitt, D. Sarkar, and N. J. Halas, "Plasmon resonance shifts of Au coated Au<sub>2</sub>S nanoshells: insight into multicomponent nanoparticle growth," *Phys. Rev. Lett.* **78**(22), 4217–4220 (1997).
6. J. B. Pendry, A. J. Holden, D. J. Robbins, and W. J. Stewart, "Magnetism from conductors and enhanced nonlinear phenomena," *IEEE Trans. Microw. Theory Tech.* **47**(11), 2075–2084 (1999).
7. M. W. Klein, C. Enkrich, M. Wegener, and S. Linden, "Second-harmonic generation from magnetic metamaterials," *Science* **313**(5786), 502–504 (2006).
8. C. Rockstuhl, F. Lederer, C. Etrich, T. Zentgraf, J. Kuhl, and H. Giessen, "On the reinterpretation of resonances in split-ring-resonators at normal incidence," *Opt. Express* **14**(19), 8827–8836 (2006).
9. C. Rockstuhl, T. Zentgraf, E. Pshenay-Severin, J. Petschulat, A. Chipouline, J. Kuhl, T. Pertsch, H. Giessen, and F. Lederer, "The origin of magnetic polarizability in metamaterials at optical frequencies - an electrodynamic approach," *Opt. Express* **15**(14), 8871–8883 (2007).
10. C. Soukoulis and M. Wegener, "Past achievements and future challenges in the development of three-dimensional photonic metamaterials," *Nat. Photonics* **5**, 523–530 (2011).
11. T. W. Ebbesen, H. J. Lezec, H. F. Ghaemi, T. Thio, and P. A. Wolff, "Extraordinary optical transmission through sub-wavelength hole arrays," *Nature* **391**(6668), 667–669 (1998).
12. F. J. García de Abajo, "Colloquium: Light scattering by particle and hole arrays," *Rev. Mod. Phys.* **79**(4), 1267–1290 (2007).
13. F. J. Garcia-Vidal, L. Martin-Moreno, T. W. Ebbesen, and L. Kuipers, "Light passing through subwavelength apertures," *Rev. Mod. Phys.* **82**(1), 729–787 (2010).
14. R. Elghanian, J. J. Storhoff, R. C. Mucic, R. L. Letsinger, and C. A. Mirkin, "Selective colorimetric detection of polynucleotides based on the distance-dependent optical properties of gold nanoparticles," *Science* **277**(5329), 1078–1081 (1997).
15. X. Huang, I. H. El-Sayed, W. Qian, and M. A. El-Sayed, "Cancer cell imaging and photothermal therapy in the near-infrared region by using gold nanorods," *J. Am. Chem. Soc.* **128**(6), 2115–2120 (2006).
16. M. L. Brongersma, J. W. Hartman, and H. A. Atwater, "Electromagnetic energy transfer and switching in nanoparticle chain arrays below the diffraction limit," *Phys. Rev. B* **62**(24), R16356–R16359 (2000).

17. D. Ricard, P. Roussignol, and C. Flytzanis, "Surface-mediated enhancement of optical phase conjugation in metal colloids," *Opt. Lett.* **10**(10), 511–513 (1985).
  18. L. Novotny, R. X. Bian, and X. S. Xie, "Theory of nanometric optical tweezers," *Phys. Rev. Lett.* **79**(4), 645–648 (1997).
  19. J. Aizpurua, P. Hanarp, D. S. Sutherland, M. Käll, G. W. Bryant, and F. J. García de Abajo, "Optical properties of gold nanorings," *Phys. Rev. Lett.* **90**(5), 057401 (2003).
  20. T. Hanke, J. Cesar, V. Knittel, A. Trügler, U. Hohenester, A. Leitenstorfer, and R. Bratschitsch, "Tailoring spatiotemporal light confinement in single plasmonic nanoantennas," *Nano Lett.* **12**(2), 992–996 (2012).
  21. P. N. Melentiev, T. V. Konstantinova, A. E. Afanasiev, A. A. Kuzin, A. S. Baturin, and V. I. Balykin, "Single nano-hole as a new effective nonlinear element for third harmonic generation," *Laser Phys. Lett.* **10** (to be published).
  22. L. D. Landau and L. P. Lifshitz, *Electrodynamics of Continuous Media* (Pergamon, 1984, Vol. 8.).
  23. X. Shi, L. Hesselink, and R. L. Thornton, "Ultrahigh light transmission through a C-shaped nanoaperture," *Opt. Lett.* **28**(15), 1320–1322 (2003).
  24. J. A. Matteo, D. P. Fromm, Y. Yuen, P. J. Schuck, W. E. Moerner, and L. Hesselink, "Spectral analysis of strongly enhanced visible light transmission through single C-shaped nanoapertures," *Appl. Phys. Lett.* **85**(4), 648 (2004).
  25. O. Lopatiuk-Tirpak, J. Ma, and S. Fathpour, "Optical transmission properties of C-shaped subwavelength waveguides on silicon," *Appl. Phys. Lett.* **96**(24), 241109 (2010).
  26. S. Link, Z. L. Wang, and M. A. El-Sayed, "How does a gold nanorod melt?" *J. Phys. Chem. B* **104**(33), 7867–7870 (2000).
  27. P. N. Melentiev, A. V. Zablotskiy, D. A. Lapshin, E. P. Sheshin, A. S. Baturin, and V. I. Balykin, "Nanolithography based on an atom pinhole camera," *Nanotechnology* **20**(23), 235301 (2009).
  28. P. N. Melentiev, T. V. Konstantinova, A. E. Afanasiev, A. A. Kuzin, A. S. Baturin, and V. I. Balykin, "Single nanohole and photoluminescence: nanolocalized and wavelength tunable light source," *Opt. Express* **20**(17), 19474–19483 (2012).
  29. L. Novotny and B. Hecht, *Principles of Nano-Optics* (Cambridge University, 2006).
  30. M. W. Klein, M. Wegener, N. Feth, and S. Linden, "Experiments on second- and third-harmonic generation from magnetic metamaterials," *Opt. Express* **15**(8), 5238–5247 (2007).
  31. M. Castro-Lopez, D. Brinks, R. Sapienza, and N. F. van Hulst, "Aluminum for nonlinear plasmonics: resonance-driven polarized luminescence of Al, Ag, and Au nanoantennas," *Nano Lett.* **11**(11), 4674–4678 (2011).
  32. P. Biagioni, D. Brida, J.-S. Huang, J. Kern, L. Duò, B. Hecht, M. Finazzi, and G. Cerullo, "Dynamics of four-photon photoluminescence in gold nanoantennas," *Nano Lett.* **12**(6), 2941–2947 (2012).
  33. P. N. Melentiev, A. E. Afanasiev, A. A. Kuzin, A. V. Zablotskiy, A. S. Baturin, and V. I. Balykin, "Single nanohole and photonic crystal: wavelength selective enhanced transmission of light," *Opt. Express* **19**(23), 22743–22754 (2011).
  34. P. N. Melentiev, A. E. Afanasiev, A. A. Kuzin, A. V. Zablotskiy, A. S. Baturin, and V. I. Balykin, "Extremely high transmission of light through a nanohole inside a photonic crystal," *Sov. Phys. JETP* **115**(2), 185–193 (2012).
  35. X. Ni, S. Ishii, M. D. Thoreson, V. M. Shalaev, S. Han, S. Lee, and A. V. Kildishev, "Loss-compensated and active hyperbolic metamaterials," *Opt. Express* **19**(25), 25242–25254 (2011).
- 

## 1. Introduction

Localized surface plasmons are nonpropagating excitations of conduction electrons of metal nanostructures which are coupled to the electromagnetic field [1–3]. The subwavelength size of nanoparticles gives rise to an efficient restoring force acting on driven electrons, which leads to the occurrence of resonances and field amplification both inside and outside nanostructures. Plasmon resonances have been studied in particles of a variety of shapes and sizes: spherical, elliptical, nanorods [2,3], nanoshells [4,5], split-ring resonators [6,7], U-shaped [8,9], and others [10]. Research by Thomas Ebbesen and colleagues [11] on an extraordinary light transmission through metal hole arrays has triggered an enormous interest in nanoholes [12,13]. According to the Babinet principle, a nanohole can be considered as a structure that is complementary to a nanoparticle and that consists of a void surrounded by a metallic medium. The possibility of using metal nanoparticles and complementary nanohole structures to manipulate light at distances far shorter than the light wavelength has opened a vast area of possible applications of these objects; thus, they can be used in chemistry and biology as sensors, in biomedical diagnostics and therapeutics, in photovoltaics, in near-field lithography and imaging, as nanowaveguides, in nonlinear optical devices, in heat-assisted magnetic recording, and as optical tweezers [14–20].

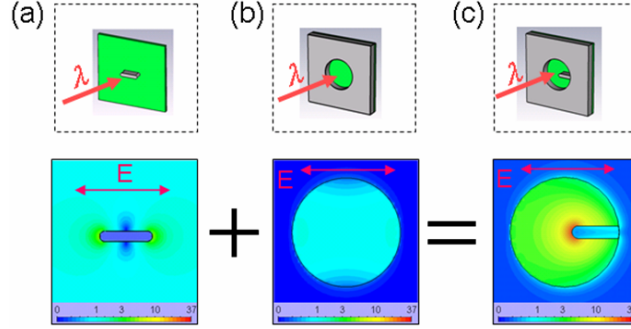


Fig. 1. The main idea of the construction of a SHR and its operation. The SHR (c) is formed from a nanorod (a) and a nanohole (b) in a metal nanofilm. Bottom: spatial distributions of the near field calculated by the FDTD method for aluminum nanostructures exposed to irradiation at a wavelength of 1560 nm: (a) a nanorod  $50 \times 180$  nm, (b) a nanohole with a diameter of 400 nm in an aluminum film 50 nm thick, (c) an SHR nanostructure formed by the nanohole (b) and the nanorod (c).

In this paper, we propose and experimentally realize a novel element for nanoplasmonics that combines a nanoparticle and a nanohole into a new nanoobject. As a particular example of such a new element, we build up a split-hole resonator (SHR) that is composed of *a nanorod and a nanohole*, as is shown in Fig. 1. One of the main merits of the marriage of the two basic elements of nanoplasmonics, the nanoparticle and the nanohole, is to realize true monopole nanoantenna for light having wavelength of the surface plasmon resonance over a large wavelength range, namely, from the UV to the IR range. The resonant wavelength of the SHR can be properly tuned by varying the SHR geometrical and material parameters. At resonance, the peak field intensity in SHR occurs at the *single* tip of the nanorod inside the nanohole. The peak field in the SHR is much stronger than the peak fields of the nanorod and nanohole, since the field in the SHR is enhanced by the following two mechanisms: the surface plasmon resonance excitation and the lightning-rod effect.

The use of SHRs in nonlinear nanoplasmonics is of special interest for the following reasons [20,21]: (i) the nanohole ensures the absence of a background from the excitation radiation, which is strongly weakened by a low transmission of the nanohole; (ii) the metal screen in which SHR is made ensures an efficient heat removal by the metal film, which, in turn, ensures the stability of the nanostructure to high-intensity radiation, making it possible to realize highly efficient nonlinear optical transformations [21]; (iii) at high intensities of the excitation field, an increase in the temperature of nanostructures does not cause a decrease in the Q factor of the plasmon resonance (resistive heating losses), because the metal film of the SHR efficiently removes heat [21]; (iv) the polarizability of a nanorod is higher than for a nanohole [22], therefore, the use of nanorods ensures a high optical nonlinearity of SHR nanostructures.

## 2. SHR nanostructure and its merits

Figure 1 illustrates the main idea of the construction of an SHR and its operation. The SHR (Fig. 1(c)) consists of a nanohole (Fig. 1(b)) and a nanorod (Fig. 1(a)) that are formed in a metal nanofilm. At the bottom of the figure, calculated distributions of the electric field amplitude in the corresponding nanostructures exposed to irradiation by a plane wave at a wavelength of  $1.5 \mu\text{m}$  are given, namely, the nanorod (Fig. 1(a)), the nanohole (Fig. 1(b)), and the SHR nanostructure (Fig. 1(c)). The wavelength of the incident radiation corresponds to plasmon resonance of the SHR nanostructure.

The calculated spatial distributions of the electric field amplitude (Fig. 1) show specific features of the SHR nanostructure. It can be seen from the spatial field distribution that the SHR forms a *monopole* antenna with the field localization near the nanorod tip. Figure 1 also shows that the maximum field strength in the SHR is an order of magnitude higher than the field magnitude for the nanorod alone (Fig. 1(a)). This occurs because the length of the

nanorod is considerably shorter than the resonant length for the selected frequency of the incident light, whereas the plasmon resonance in the nanorod arises only if its length is approximately equal to a half of the plasmon wavelength. Therefore, the geometry of the SHR makes it possible to realize plasmon resonance *at smaller linear geometric dimensions* of the nanostructure.

Among known nanostructures, there is particular one that has geometry similar to SHR. It is C-shaped aperture [23–25]. The geometry of C-shaped aperture is optimized to realize high level of transmission, while SHR geometry is optimized to have one and only one maxima of electric field located at the end of SHR nanorod. Comparison of the SHR with other known *monopole* nanoantennas (dual nanodisks, bow-tie nanoantennas, etc.) shows that, other conditions being equal, the SHR nanostructure (as an antenna) has *smaller geometric dimensions* for the plasmon resonance to arise, since only single resonant nanostructure is used to form SHR monopole antenna, while in monopole antennas of other type at least two resonant nanostructures are used. A smaller physical volume of the nanoantenna is of great practical importance. Thus, the generation efficiency of the third harmonic by an antenna of a smaller size is considerably higher, which is related to longer plasmon damping times in the nanoantenna of a smaller physical volume [20].

An SHR, as many other nanostructures, can be considered as a nanolocalized radiation source. From this viewpoint, the SHR also has a number of merits. First, there is no accompanying background of the excitation radiation, which is commonly very high and is always present when dealing with nanoobjects in the form of nanoparticles. Second, the transmission of the radiation through the SHR is significantly higher than through the nanohole of the same size. Third, since the SHR is created in a metal film, it is capable of withstanding a higher intensity of the radiation incident on it than isolated nanoparticles [21,26], and, correspondingly, as a nonlinear element, can be more efficient in the transformation of the radiation.

### **3. Creation of a SHR and investigation of its optical and spectral characteristics**

As a material for the creation of an SHR, we used aluminum. Investigations of SHRs were performed using radiation at a wavelength of 1560 nm, since at this wavelength, aluminum is characterized by strong optical nonlinear properties; thus, the optical nonlinearity coefficient  $\chi^{(3)}$  of aluminum is approximately 1000 times higher than that of gold [21]. In addition, the radiation at 1560 nm is widely used in modern telecommunication systems. The SHR nanostructures with the geometry shown in Fig. 1(c) were formed using a focused ion beam in an aluminum film 200 nm thick and their nanohole diameter - 380 nm.

We examined the optical and spectral properties of SHR nanostructures. In experiments, SHRs were irradiated by pulsed laser radiation ( $\tau = 120$  fs) with a power of 15 mW, which was focused into a spot with a diameter of 4.5  $\mu\text{m}$ . All measurements were performed with individual SHRs. We studied nonlinear optical processes such as the third-harmonic generation (THG) and multiphoton photoluminescence.

The experimental setup is schematically shown in Fig. 2. SHR nanostructures were irradiated by a femtosecond fiber laser (wavelength 1560 nm, pulse duration 120 fs, pulse repetition rate 70 MHz, mean radiation power incident on the sample with SHR - 15 mW). The optical and spectral properties of SHR were measured using an inverted microscope

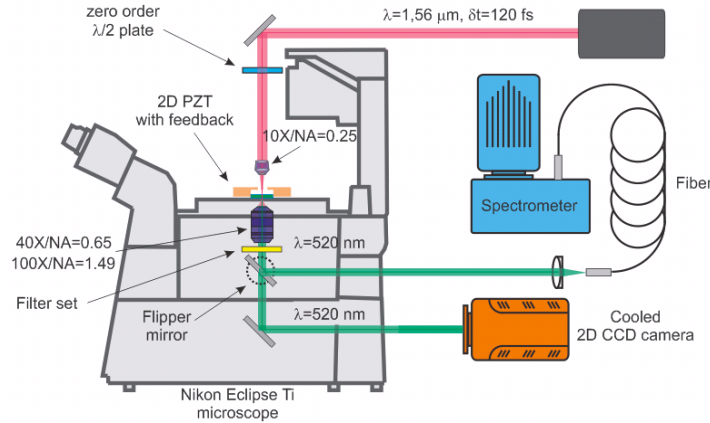


Fig. 2. Schematic of the experimental setup for investigation of SHR nanostructures.

(Nikon Eclipse Ti/U). The laser radiation, focused by an objective (10x, NA = 0.25) into a spot  $4.3 \mu\text{m}$  in diameter, was directed transversely to the surface of a film with SHR nanostructures. The peak radiation intensity on the sample was on the order of  $1.1 \times 10^{10} \text{ W/cm}^2$ . A zero-order  $\lambda/2$  phase plate was used to control the polarization of the incident radiation. The scattered radiation from SHR was collected with objectives 40x, NA = 0.65, or 100x, NA = 1.49. A set of interference and color filters was used to suppress the excitation radiation. The radiation at the fundamental frequency was collected with a lower efficiency because of the chromatic aberration of the objective lens, which becomes considerable at a large difference between the wavelengths of the fundamental radiation and the third harmonic. Finally, the radiation at the fundamental frequency was suppressed by more than 13 orders of magnitude. Details of measurement of THG signal from a single nanostructure can be found elsewhere [21].

SHR nanostructures under investigation were prepared in 200-nm thick Al films that were deposited on the surface of ultrathin (40 nm thick)  $\text{SiO}_2$  membranes with a low roughness ( $<1.5 \text{ \AA}$ ) [27], which, in turn, led to a low roughness of metal films adjacent to the membrane. A high quality of the metal surface greatly reduced the contribution of luminescence from roughness of the metal surface to the signal being detected [28]. For this reason, in all the measurements, the smooth side of films was exposed to the radiation at the fundamental frequency.

Aluminum films were formed by e-beam evaporation. The thickness of the films was measured by an atomic force microscope using the razor blade scratch technique and was determined to be  $200 \pm 25 \text{ nm}$ . The roughness of Al film surface side adjacent to  $\text{SiO}_2$  membrane is less than 1 nm. The measured roughness of the other Al film surface side is as follows: the height roughness (RMS) is about 1.5 nm, and the lateral roughness (correlation length) is about 5 nm. The samples were prepared under the conditions of Class 100 cleanroom; their optical measurements were performed under the conditions of Class 1000 cleanroom. To prepare a SHR nanostructures, we used a  $\text{Ga}^+$  beam, 30 keV (FEI Quanta 3D), focused on the Al film surface into a spot with a diameter of about 10 nm. Microscopy of SHR nanostructures were conducted by a JEOL JSM-7001F electron microscope, whose spatial resolution is about 5 nm. To diminish the carbon deposition during the electron beam microscopy experiments, the measurements were carried out at relatively low electron beam energy of about 5 keV. To prevent the influence of plasmonic collective effects, the spacing between SHR nanostructures was not less than  $5 \mu\text{m}$ . This spacing also exceeds the spot diameter of the laser beam. The order in which the SHR are arranged permit us to identify each of them using the optical microscope and to work with them individually. The geometry of the SHR nanostructure was optimized based on calculations of resonant properties of the nanostructure.

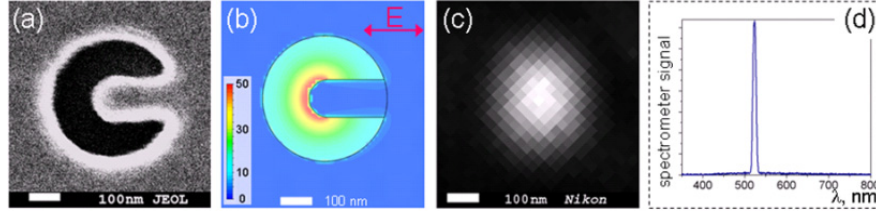


Fig. 3 . Generation of the third harmonic by an SHR nanostructure formed in aluminum film. (a) an electron microscope image of the nanostructure formed by a nanohole of 380 nm diameter and nanorod of 220 nm (length)  $\times$  120 nm (width), (b) calculated enhancement of the electric field amplitude upon irradiation of the nanostructure of Fig. 3(a) by a plane monochromatic wave with a wavelength of 1560 nm, (c) an optical image of the nanostructure upon its laser irradiation at a wavelength of 1560 nm and detection at the THG wavelength, and (d) measured spectrum of radiation that forms optical image presented on Fig. 3(c) . The incident radiation is polarized along the direction of the nanorod of the nanostructure.

#### 4. Third-harmonic generation

Figure 3 presents measurement results for the THG from a single SHR nanostructure. The calculated spatial distribution of the electric field amplitude for the nanostructure irradiated by a plane monochromatic wave is shown in Fig. 3(b). It can be seen that the spatial distribution of the electric field amplitude at the fundamental frequency has a clearly pronounced maximum and is localized inside the SHR nanostructure near the tip of its nanorod (Fig. 3(b)). In turn, this field acts as a source of a third-order polarization, which results in the THG. It can be seen from the figure that the spatial localization of the third-harmonic radiation source is determined by the size of the nanorod tip, which is about 100 nm. In the optical image of the nanostructure (Nikon Ti/U inverted microscope) obtained at the wavelength of the third harmonic, a diffraction-limited spot is seen, the width at half-height of which is about 230 nm (Fig. 3(c)). An elliptical shape of this spot indicates that the detected radiation is polarized in the direction orthogonal to the polarization of the excitation radiation [29]. Measurements of the emission spectrum of the SHR nanostructure show that it consists of a narrow line located at the frequency of the third harmonic of the excitation radiation (Fig. 3(d)).

Our measurements and calculations showed that the THG efficiency of the SHR nanostructure strongly depends on its geometry (the nanostructure diameter, the nanorod length, the film thickness), the material of the film, and the refractive index of the medium surrounding the SHR. This behavior is explained by the well-known strong dependence of the excitation efficiency of localized plasmon oscillations on the geometry of the nanostructure and its local environment [13], which determines the distribution and amplitude of the electromagnetic field near the nanostructure. Our study of the influence of the nanostructure geometry on the THG efficiency reveals that there is a strong resonant behavior of the dependence of the THG on the diameter of the SHR nanohole and on the length of its nanorod.

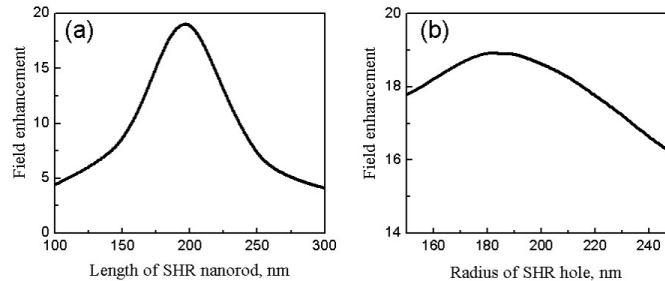


Fig. 4. FDTD calculations of electric field amplification at fundamental frequency in the vicinity of end of a SHR nanorod for various geometry of SHR with a fixed 120 nm width of a

nanorod: (a) SHR with fixed radius is equal to 185 nm and different length of its nanorod, (b) SHR with fixed length of its nanorod is equal to 190 nm and different radius of its hole.

Figure 4 presents our calculations of electric field amplification at fundamental frequency in the vicinity of end of SHR nanorod for various geometry of SHR. Calculations were made with use of the finite-difference time-domain method (FDTD, precision is about  $10^{-6}$ ) for a plane monochromatic wave excitation at wavelength  $1.56 \mu\text{m}$  impinging on SHR made in 200 nm thick Al film. From Fig. 4 it can be seen that the electric field amplification has a resonant behavior both on length of SHR nanorod (Fig. 4(a)) and on radius of SHR hole (Fig. 4(b)). By analogy with U-shaped nanostructures [8], this resonant behavior can be interpreted as follows. A plasmon wave propagates in the nanostructure along the metal/dielectric boundary, which is formed by the nanohole perimeter of the SHR nanostructure. The nanorod plays a role of mirrors which reflect the plasmon wave. If the perimeter length of the hole that forms a nanostructure is equal to an integer number of half-waves of the plasmon wave, then resonances of the Fabry–Perot type are excited in the nanostructure. The length of the SHR nanorod determines the reflection coefficient and the phase shift of the plasmon wave.

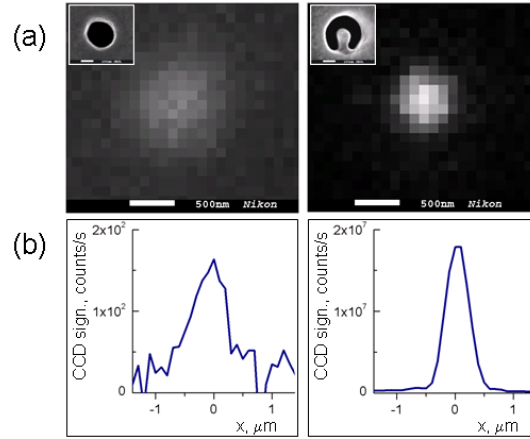


Fig. 5. Third harmonic generation by a single nanohole with a diameter of 200 nm (left) and an SHR nanostructure (right) that have equal open surface areas: (a) two-dimensional optical microscope images of the nanostructures at the THG frequency (the electron microscope images of the nanostructures are presented as insets), and (b) corresponding transverse sections of the optical images. The nanostructures were prepared in an aluminum film 200 nm thick.

We measured the efficiency of THG from two different types of nanostructures: (i) a nanohole with a diameter of 200 nm and (ii) an SHR nanostructure (Fig. 5). Electron microscope images of these nanostructures are shown in Fig. 5(a), while their optical microscope images at the THG frequency are given in Fig. 5(b). Both nanostructures have approximately equal open surface areas; however, as our measurements showed, the transformation efficiency of the radiation into the third harmonic is almost *five orders of magnitude* higher for the SHR nanostructure than for the single nanohole (Fig. 5(b)).

The efficiency of THG was determined using the following expression [21]:

$$\eta_{THG} = \frac{1}{\kappa} \frac{P_{THG}}{I(\omega) \times S_{hole}}, \quad (1)$$

where  $\kappa$  is the efficiency of the radiation collection by the objective ( $\kappa = 0.24$  for the 40x objective,  $\kappa \approx 1$  for the 100x objective),  $P_{THG}$  is the detected power of the third-harmonic radiation from the nanohole,  $I(\omega)$  is the radiation intensity at the fundamental frequency, and  $S_{hole}$  is the nanohole area. The absolute value of the transformation efficiency of the excitation radiation into the third harmonic per unit area (the intensity ratio of the third-

harmonic radiation and the radiation at the fundamental frequency) is about  $10^{-5}$ , which is a record high value for experiments on the THG from single nanostructures. Up to now the maximum conversion efficiency of THG was realized on nanostructures in a shape of a splitting resonator [30]. The absolute value of THG efficiency for single split-ring resonator nanostructure was as high as  $3 \times 10^{-7}$ .

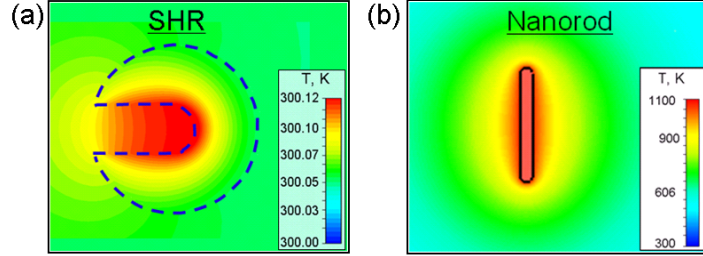


Fig. 6. (a) Calculated 2D spatial temperature distribution in an SHR nanostructure (formed by a nanohole with diameter of 380 nm and nanorod of 220 nm (length)  $\times$  120 nm (width), made in 50 nm thick Al film) exposed to femtosecond laser radiation (wavelength 1560 nm, pulse duration 120 fs, pulse repetition rate 70 MHz) with a peak intensity of  $5 \times 10^{11}$  W/cm<sup>2</sup>. Blue dashed line shows the contour of the SHR nanostructure. (b) Calculated 2D spatial temperature distribution in Al nanostructure made in a form of a nanorod of size 50 nm  $\times$  50 nm  $\times$  570 nm arranged on a SiO<sub>2</sub> substrate and exposed to the femtosecond laser radiation with a peak intensity  $5 \times 10^{11}$  W/cm<sup>2</sup>.

It is worth noting that a 50-fold increase in the intensity of the excitation radiation (to a value of  $I = 5 \times 10^{11}$  W/cm<sup>2</sup>) should lead to an increase in the THG efficiency to a value that is close to unity. Below we will show that, at this intensity of the incident radiation, there is no destruction of the nanostructure by thermal. A maximal temperature on the surface of the SHR nanostructure does not exceed 300 K, which is considerably lower than the melting temperature of the nanostructure. We also note that this radiation intensity is below the destruction threshold of the metal due to the plasma formation under the action of intense femtosecond radiation. Therefore, the SHR nanostructure is a good candidate for the creation of a nanolocalized source of THG with efficiency close to unity.

Figure 6 shows the temperature distribution in an SHR nanostructure in a 50-nm thick Al film that was determined by numerical solving of heat conduction equations by the FDTD method. The temperature distribution corresponds to the state of thermodynamic equilibrium of nanostructures impinged by the laser light. Figure 6(b) shows a spatial temperature distribution in an aluminum nanorod of size 50 nm  $\times$  570 nm arranged on a SiO<sub>2</sub> substrate. The heating occurs due to the absorption of the excitation radiation. The structures are exposed to a Gaussian laser beam with a diameter about 4.5  $\mu$ m, the wavelength is 1560 nm, and the wave vector is orthogonal to the nanostructure plane. The radiation intensity is  $5 \times 10^{11}$  W/cm<sup>2</sup>. The polarization was directed to excite the plasmon resonance for in both nanostructures. It can be seen from the figure that temperature of the SHR nanostructure is very close to room temperature ( $\sim$ 300 K), while the nanorod is heated to much higher temperature ( $\sim$ 1100 K) with the radiation intensities being the same. These calculations show that it is impossible to use nanorod at high radiation intensities (due to its destruction) which, in its turn, means that the efficiencies of THG on such object will differ drastically.

## 5. Multiphoton luminescence

Multiphoton *luminescence* is a consequence of the excitation of surface electron states that are localized on the metal surface and that arise on nanosized inhomogeneities of the aluminum film surface [31,32]. To excite multiphoton luminescence in an SHR, we formed nanosized inhomogeneities at the tip of its nanorod, where a maximal intensity of the field at the

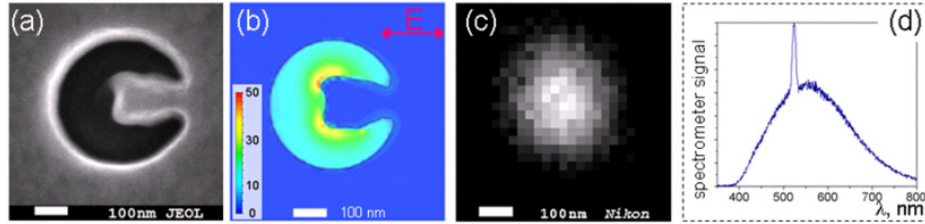


Fig. 7. Multiphoton photoluminescence from a SHR nanostructure formed in an aluminum film. (a) an electron microscope image of the nanostructure formed by a nanohole of 380 nm diameter and nanorod of 220 nm (length)  $\times$  120 nm (width), (b) calculated enhancement of the electric field amplitude inside the SHR of Fig. 7(a) upon irradiation of the nanostructure by a plane monochromatic wave with a wavelength of 1560 nm, (c) an optical image of the nanostructure upon its laser irradiation at a wavelength of 1560 nm and detection in the spectral range 400–800 nm, and (d) measured emission spectrum of multiphoton luminescence.

fundamental frequency is observed. The inhomogeneities were created with an ion beam (FEI Quanta 3D), and their size was in the range 5 – 15 nm (Fig. 7). The remaining geometric dimensions of the SHR with inhomogeneities were the same as those of the “smooth” SHR nanostructure presented in Fig. 3. Our calculations showed that the optical linear properties of this nanostructure (light transmission and scattering) do not differ from the optical properties of the nanostructure that has the smooth nanorod.

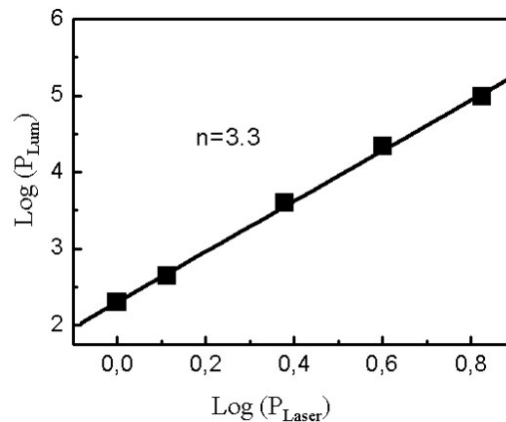


Fig. 8. Experimental measurements of dependence of a multiphoton photoluminescence power from a SHR nanostructure formed in an aluminum film as a function of power of excitation laser field.

This “inhomogeneous” SHR nanostructure illuminated by radiation with the same parameters as the nanostructure of Fig. 3. Figure 7 presents results of our investigations on the generation of multiphoton luminescence by the single SHR nanostructure with surface irregularities. The calculated field distribution of the nanostructure is shown in Fig. 7(b). It can be seen from this figure that the spatial distribution of the field at the fundamental frequency exhibits a clearly pronounced maximum near the tip of the SHR nanorod. The optical observation of the SHR with an optical microscope (Nikon Ti/U with a 40x/0.65 objective) at the luminescence wavelength yields an image of the nanostructure in the shape of a diffraction-limited spot (Fig. 7(c)). It can be seen from the figure that, as distinct from the optical image shown in Fig. 3(c), this spot has a circular shape, which indicates that the luminescence radiation is depolarized. The emission spectrum of the SHR nanostructure consists of a narrow peak, which corresponds to the third harmonic of the excitation radiation, and a broad radiation band, which covers the spectral range from 390 nm to longer than 800 nm (Fig. 7(d)). Power scaling of the photoluminescence signal is shown in Fig. 8. The

measured data points are plotted on a log-log scale and fit to a linear equation with slopes of 3.3. Thus intensity dependence measurements show that this broadband radiation is a result of three and four photon photoluminescence processes.

In nanoplasmonics, resonance frequencies of plasmon oscillations of a nanostructure and, as a consequence, its optical properties are substantially determined by its size and shape. In most cases to create a nanostructure with predetermined optical properties, its geometry should be controlled with an accuracy of about  $\lambda/10$ . Dramatic changes in the spectrum of the nonlinear optical response in the SHR with a change in its geometry that were presented above convincingly show that, in the nonlinear nanoplasmonics, the nanostructure geometry should be controlled with an accuracy considerably better than  $\lambda/100$ .

## **6. Conclusion**

In a conclusion, we have realized giant optical nonlinearity of a single nanostructure which we call a split hole resonator: (i) it allows a record high efficiency of generation of the third harmonic of radiation from a single nanostructure; (ii) it allows a record high efficiency of generation of multiphoton luminescence; (iii) it makes it possible to realize a nanolocalized radiation source with a spatial localization of about  $\lambda/15$ . We also note that it is possible to further increase the operation efficiency of SHR nanostructures using microcavities based on photonic crystals [28,33,34] or active hyperbolic metamaterials [35].

## **Acknowledgments**

This work was partially supported by the Russian Foundation for Basic Research, by the Program «Extreme Light Fields» of the Presidium of the Russian Academy of Sciences, and by the Ministry of Education and Science of the Russian Federation. This work was produced using equipment of ISAN Center of Collective Use and MIPT Center of Collective Use with the financial support from the Ministry of Education and Science of the Russian Federation (contract № 16.552.11.7070).